A 561-yr (1461-2022 CE) summer temperature reconstruction for Mid-Atlantic-Northeast USA shows connections to volcanic forcing and atmospheric circulation

Grant L. Harley[1] · Justin T. Maxwell[2] · Karen E. King[3] · Shelly A. Rayback[4] ·
Edward R. Cook[5] · Christopher Hansen[6] · R. Stockton Maxwell[7] · Frederick Reinig[8] ·
Jan Esper[8,9] · Tsun Fung Au[10,11] · Ellen V. Bergan[1] · Katherine E. Brings[1] ·
Nick Koenig[1] · Benjamin Lockwood[12] · Richard D. Thaxton[1]

Abstract
Contextualizing current increases in Northern Hemisphere temperatures is precluded by the short instrumental record of the past *ca.* 120 years and the dearth of temperature-sensitive proxy records, particularly at lower latitudes south of $<50\,°N$. We develop a network of 29 blue intensity chronologies derived from tree rings of *Tsuga canadensis* (L.) Carrière and *Picea rubens* Sarg. trees distributed across the Mid-Atlantic and Northeast USA (MANE)—a region underrepresented by multi-centennial temperature records. We use this network to reconstruct mean March-September air temperatures back to 1461 CE based on a model that explains 62% of the instrumental temperature variance from 1901−1976 CE. Since 1998 CE, MANE summer temperatures are consistently the warmest within the context of the past 561 years exceeding the 1951−1980 mean of +1.3 °C. Cool summers across MANE were frequently volcanically forced, with significant ($p<0.05$) temperature departures associated with 80% of the largest tropical (n=13) and extratropical (n=15) eruptions since 1461 CE. Yet, we find that more of the identified cool events in the record were likely unforced by volcanism and either related to stochastic variability or atmospheric circulation via significant associations ($p<0.05$) to regional, coastal sea-surface temperatures, 500-hpa geopotential height, and 300-hpa meridional and zonal wind vectors. Expanding the MANE network to the west and south and combining it with existing temperature-sensitive proxies across North America is an important next step toward producing a gridded temperature reconstruction field for North America.

1 Introduction

Over the 20th century, mean annual surface air temperatures in the eastern United States (US) have risen by more than 1 °C and are projected to continue increasing throughout this century (Kunkel et al. 2013; Horton et al. 2014; Vose et al. 2017). Regionally, the Mid-Atlantic to Northeast region of the US (hereafter MANE) has experienced a 2 °C increase in mean

---

Extended author information available on the last page of the article

annual temperatures since 1960 (Vose et al. 2017). Although broad-scale reconstructions of temperature across the high latitudes of Northern Hemisphere show strong, multidecadal synchrony from multiple proxy sources (Wilson et al. 2016; Neukom et al. 2019a), an improved understanding of the coherence between more regional-scale temperature records with broad-scale reconstructions is needed for more accurate climate simulations (Neukom et al. 2019b), especially at lower- to mid-latitude locations.

Reconstruction of climate variability, particularly temperature, across the mid-latitudes of the eastern US has been challenging due to the land-use history and ecology of eastern forests which leaves few old trees on the landscape with which to build proxy records. In the eastern US, there are three primary tree species known to exhibit sensitivity to temperature: *Chamaecyparis thyoides* L. (Atlantic white cedar), *Tsuga canadensis*(L.) Carrière (eastern hemlock), and *Picea rubens* Sarg. (red spruce). *C. thyoides* for instance, displays a temperature signal extending from winter to summer (Pederson et al. 2004; Hopton and Pederson 2005). Pearl et al. (2017) developed a mean January-August temperature reconstruction for the northeast US based on *C. thyoides* ring-width chronologies that explained 34% of the instrumental variance. By increasing the number of sites, Pearl et al. (2020b) expanded on their earlier efforts and produced a more robust spatial temperature field reconstruction for New England, but the temperature record, based exclusively on *C. thyoides*, only extends to the *ca.* 1820s. *T. canadensis*, on the other hand, has been shown to contain a strong prior- and current-year temperature signal and is a broadly distributed, low elevation (*e.g.* <400 m), and long-lived (>400 years) species in eastern North America (Cook and Cole 1991; Tardif et al. 2001; Maxwell et al. 2020; Stern et al. 2021; Harley et al. 2021). Finally, *P. rubens* is a shade-tolerant conifer that can live for more than 300 years. Previous studies show *P. rubens* from the Northeast US to be sensitive to spring (Apr−May) temperature variability (Conkey 1986; Sheppard et al. 1996; Kosiba et al. 2018). The core distribution of *P. rubens* is in northeastern US and Canada but is also found in small, disjunct populations in the southern Appalachian Mountains of eastern Tennessee, western North Carolina, and northern Georgia. The so-called *spruce zone*—where *P. rubens* attains its maximum importance as a primary producer in the spruce-fir community—varies across its geographic range by elevation, with individuals positioned within a wider elevation envelop in the northern part of its range <650−>950 m asl (Foster and D'Amato 2015; Kosiba et al. 2018), but only found at elevations >1400 m asl at southern range margins (McLaughlin et al. 1987).

A concerted effort has been made over the past few decades to establish a network of high-resolution temperature proxy records throughout the Northern Hemisphere to gauge temperature variability (Esper et al. 2002; Frank et al. 2007; Wilson et al. 2007; Jones et al. 1998; Mann et al. 1999, 2009; Wahl and Ammann 2007). With the recent formation of the Northern Hemisphere Tree-Ring Network Development (N-TREND), this consortium aims to define a collective strategy for improving large-scale summer temperature reconstructions from new and existing tree-ring chronologies (Wilson et al. 2016). Currently, most N-TREND records are located at higher latitudes (>50 °N), thus, substantial spatial gaps exist in the North American region of the N-TREND network (Anchukaitis et al. 2017). In particular, the MANE region is underrepresented due to a lack of temperature-sensitive tree-ring records. Since the creation of the N-TREND network, advances in dendrochronological techniques such as blue intensity (McCarroll et al. 2002) have demonstrated the ability to provide robust paleotemperature estimates at the mid-to-lower latitudes across many regions of the Northern Hemisphere (Heeter et al. 2019, 2020, 2021; Cao et al. 2022; Zheng et al. 2023). In North America, recent work has demonstrated the promising potential of using BI methods to improve the spatial gaps in the North American paleotemperature record over the eastern US and Canada (Wang et al. 2022; Harley et al. 2021).

As rising temperatures and heat waves increase stress on natural and human systems, particularly in a region of the US where >72 million people live, a better understanding of the historical context of current summer warmth in the eastern US requires more accurate estimations of past trends and drivers of summer temperatures. Building upon the work of Harley et al. (2021), we expand and evaluate the pre-existing network of latewood blue intensity (LWBI) data from *T. canadensis* and *P. rubens* trees to develop a regional-scale reconstruction of summer temperatures for the MANE region of the US. Using this network, we addressed the following research questions: [1] Is the rate of warming across the MANE region since *ca.* 1960 unprecedented within the context of the past *ca.* 500 years? [2] What is the full range of pre-instrumental temperature variability for MANE? [3] What are the natural and anthropogenic forcings on temperature over the last *ca.* 500 years?

2 Data and methods

2.1 Tree-ring network

Spanning a latitudinal range from Maryland to Maine (Fig. 1), tree-ring data for the reconstruction are sourced from two conifer species in the eastern US that are suitable for BI (Heeter et al. 2019; Harley et al. 2021): *T. canadensis* and *P. rubens*. First, the majority of the MANE LWBI network is comprised of preexisting *T. canadensis* samples collected during the 1970s and 1980s by Cook and Cole (1991), who targeted the oldest known stands across much of the species' range in the US. Many of these site collections from the original study have since succumbed to logging or other disturbances (*e.g.* physical, biological); hence, the physical cores from these collections are arguably priceless within the context of this study and broader dendrochronological archives. In October 2020, we obtained the original collections from the wood archive at Columbia University's Lamont-Doherty Earth Observatory Tree-Ring Lab. We selected collections with the greatest length and sample replication back in time, specifically targeting collections that extended before 1600 CE. Further making use of preexisting collections, we obtained physical samples cored in 2012−2013 by Belmecheri et al. (2021), which comprised multiple recollections of the same sites cored in the 1970s and 1980s by Cook and Cole (1991), as well as new site collections.

Supplementing the reprocessing of existing collections for BI, we conducted a series of additional recollections during the summers spanning 2019−2021 at several of the Cook and Cole (1991) and Belmecheri et al. (2021) sites, as well as collected two new sites (Swallow Falls, Maryland and Nancy Brook, New Hampshire) in summer 2021. At each of the 2019−2021 new and recollection sites, we gathered two cores from 20−30 trees with handheld increment borers. Tree cores were prepared following protocols detailed by Harley et al. (2021). For all preexisting collections, all physical samples were re-sanded, scanned, measured, and visually crossdated using the same procedure detailed above. For each site, we measured total ring width using the CooRecorder program (Larsson 2014). We statistically validated visual crossdating for all site collections using the total ring width series and the xDater Shiny application (Bunn 2008, 2010). Once each site collection was absolutely dated, we collected LWBI from all samples in CooRecorder. For each site, we used the Signal Free detrending program (https://www.geog.cam.ac.uk/research/projects/dendrosoftware/) to standardize all tree-ring series using the signal-free standardization (Melvin and Briffa 2008) in which the base curve was a smoothing spline with an amplitude response of 0.50 at a period associated with 67% of each series length (Cook and Peters 1981). This method was chosen to retain as much climate signal as possible while removing non-climatic sig-
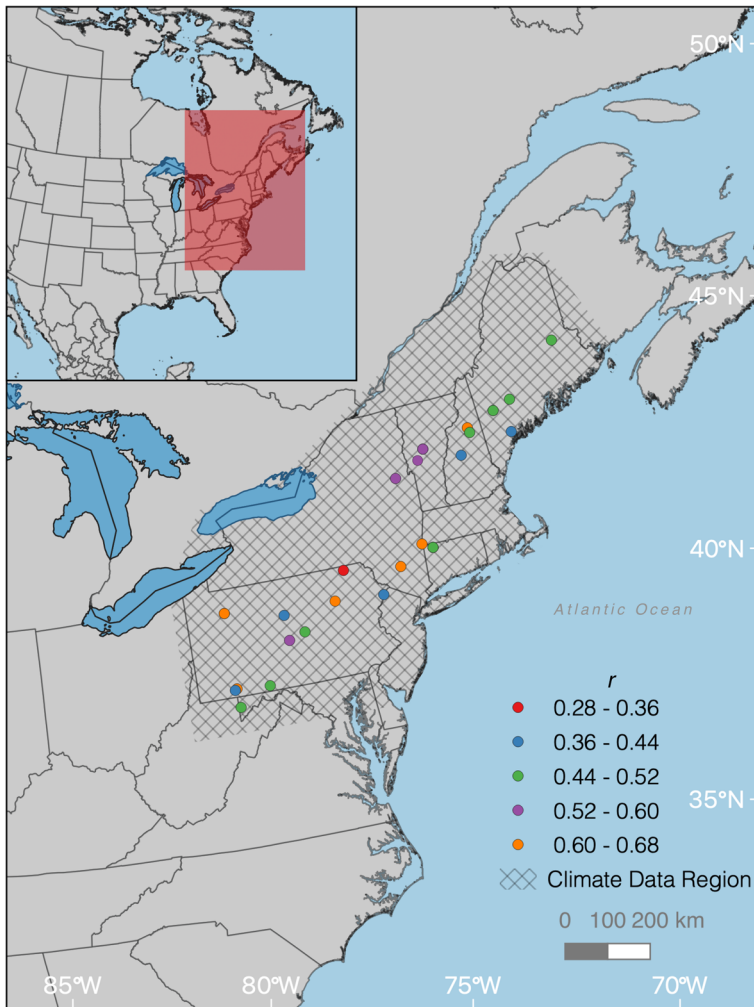
Fig. 1 The MANE network consists of 29 LWBI chronologies, all of which were used as predictors in the $T_{Mar-Sep}$ reconstruction. Map showing predictor chronology locations (circles) and target instrumental data (hatch) gathered from the CRU TS4.07 0.5°$T_{Mar-Sep}$ field (Harris et al. 2020) during the period 1901−1976. Colors indicate Pearson correlations ($p<0.05$) with the target instrumental data averaged over the hatched region

nal related to disturbance and age-related tree-ring growth trends. To account for the effect of diminishing sample size back through time, we applied variance stabilization during the standardization process and then truncated each chronology where the expressed population signal statistic fell below a threshold of 0.80 (Wigley et al. 1984; Maxwell et al. 2017).

2.2 Instrumental temperature data

We relied on previous results from Harley et al. (2021) in which the association between instrumental temperature and site LWBI chronologies at five *T. canadensis* and one *P. rubens* sites (all of which are included in this study) and found mean temperatures from

March-October ($T_{Mar-Oct}$) to be the most robust predictor of LWBI variability. A principal components analysis (PCA) amongst all sites revealed PC_1 to account for 39% of the cumulative proportion of variance. We noticed that including T_{Oct} resulted in weaker associations contrary to Harley et al. (2021); $T_{Mar-Sep}$ resulted in the strongest predictor of PC_1 (Fig. 2). We used PC_1 to identify the climatic footprint of the network by conducting a spatial Pearson's correlation between PC_1 and the CRU TS4.07 monthly mean air temperature field (Harris et al. 2020) during the period 1901−1976, the common period of overlap amongst all sites. Mapping the area of highest correlation (r=0.6+, p<0.05) space between PC_1 and the gridded spatial temperature field revealed a broad climate footprint across the eastern US (Mid-Atlantic, Northeast, and Midwest) and south-eastern Canada (Fig. S4). However, given the lack of predictor BI chronologies from the Midwest US and south-eastern Canada, we elected to be more conservative with our target instrumental temperature data. Thus, we averaged $T_{Mar-Sep}$ data from the CRU TS4.07 field within the vicinity of our predictor chronologies across the MANE region (hatched area in Fig. 1 corresponding to the region bound by the following: (47.60°N,68.70°W; 44.80°N,67.01°W; 38.91°N,75.32 °W; 39.26 °N,80.38 °W; 43.32 °N,80.35°W).

2.3 Reconstruction model

We reconstructed estimates of regionalized summer air temperature using a nested principal components regression (PCR) model, which accounts for the decrease in the number of predictor chronologies back through time (Cook et al. 1999, 2004, 2007). During the initial screening phase, we prewhitened both the LWBI predictors and instrumental data to ensure independence before modeling to meet the assumptions of normality (Cook and Peters 1997). LWBI chronologies from the initial candidate pool were retained for PCR modeling if they contained positive and significant correlations (p<0.10 for Pearson's, Spearman, and Robust Pearson's tests) with the predictand data over the common period of overlap amongst all predictors in the candidate pool (1901-1976). Following the Kaiser-Guttman rule (Guttman 1954; Kaiser 1960), the first n eigenvectors with eigenvalues >1 were retained for the multiple regression. The final subset of PCs in the regression model was determined by considering the minimum Akaike information criterion (AIC), which includes a penalty term for increasing the number of predictors in the model (Akaike 1974). The first model was calibrated for the common period of all chronologies (1901-1976) with the target instrumental data. Successive
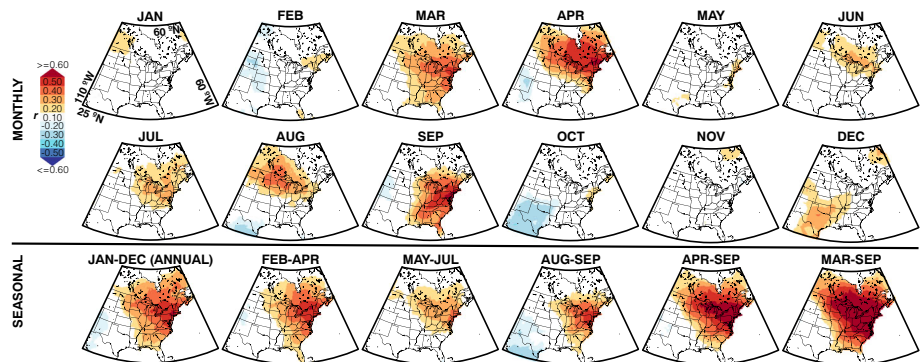

Fig. 2 $T_{Mar-Sep}$ **provided the strongest signal across the MANE LWBI network.** Monthly (top) and seasonal (bottom) correlations (Pearson's r; p<0.05; 1st-differenced) between PC_1 of the MANE BI network and $T_{Mar-Sep}$ (Harris et al. 2020) during the period 1901−1976

models were calculated backward in time intervals based on chronology length, with fewer chronologies as they dropped out. Similarly, forward nests were calculated in intervals based on when the most recent chronologies ended to include more recent tree-ring collections.

To validate each backward- and forward-nested reconstruction model, we split the common period ($1901-1976$) into two equal periods for calibration ($1939-1976$) and verification ($1901-1938$). To ensure each model was time stable, we calculated validation statistics for models calibrated on the "late" period ($1939-1976$) and verified on the "early" period ($1901-1938$), as well as flipped to calibrate on the early and verify on the late. We performed model validation by calculating two goodness-of-fit tests: the reduction of error (RE) and coefficient of efficiency (CE) (Fritts 1976; Cook et al. 1999). The validation statistics produced were the calibration and verification period coefficient of determination and the verification period reduction of error and coefficient of efficiency. We produced the final reconstruction by calibrating on the full common period. After each nest was calculated, temperature estimates along with each set of calibration and verification statistics were spliced together for the entire reconstruction length. Finally, we used the methods of Robeson et al. (2020) to bias-correct the reconstruction to the target instrumental data using a quantile mapping approach based on localized linear regression (Fig. S1).

2.4 Volcanic forcing

We used a double-bootstrapped approach to applying superposed epoch analysis (SEA; Rao et al. 2019) to investigate the MANE $T_{Mar-Sep}$ response to global-scale volcanic eruptions since 1461 CE. We first build a list of eruption years for tropical and extratropical volcanic events (Table S1) based on the stratographic aerosol optical depth at 550 nm from the eVolv2k reconstruction from Toohey and Sigl (2017) during the period $1461-1900$, which is the period of overlap with the MANE reconstruction. We also include global-scale, instrumental-period eruptions of 1912 (Novarupta), Agung (1963), 1982 (El Chicon), and 1991 (Pinatubo) from the Global Volcanism Program Volcanoes of the World database (v.5.1.7). In total, we used SEA to test for significant ($\alpha=0.05$) MANE $T_{Mar-Sep}$ departures for the period 5 years before and 15 years following a total of 28 events, 13 tropical and 15 extratropical eruptions. Statistical significance and uncertainty were calculated using the random bootstrapping method with 10,000 iterations (Rao et al. 2019).

2.5 Reconstruction assessment

We characterize past temperature variability using a severity-duration analysis (González and Valdés 2003) of reconstructed $T_{Mar-Sep}$ values. This analysis quantifies the magnitude (average cumulative departure from the long-term mean), duration (period of each event), and intensity (duration divided by the magnitude) of anomalously warm and cool events. Here, we considered an 'event' to be any warm or cool period spanning at least two consecutive years. To better understand linkages with upper-level atmospheric dynamics, we compared our temperature reconstruction to the following gridded atmospheric products: 300-hpa zonal and meridional wind stress (Compo et al. 2011) and 500-hpa geopotential height from 20th Century Reanalysis V3 during the period $1836-2021$ (Compo et al. 2011), and instrumental sea surface temperature (SST) from HadISST 1°reconstruction during the period $1870-2021$ (Rayner et al. 2003). Finally, we compare the MANE $T_{Mar-Sep}$ record [1] with an instrumental temperature record from New Haven, Connecticut since 1781 and [2] with numerous other reconstructions of summer/warm-season temperatures from across North America from

the following: Eastern Canada MJJA T_{mean} (Wang et al. 2022)(MXD); Pacific Northwest USA/southwestern Canada JJA T_{mean} (Heeter et al. 2023) (BI); and Southeast USA AS T_{max} (BI) (King et al. In Press). We plot 30-year smoothed versions of each reconstruction as z-scores relative to the mean and standard deviation over the period 1951−1980 CE. Pearson's correlations tested at the $p<0.05$ level between each of the reconstruction time series are calculated over the common period of all reconstructions.

3 Results and discussion

3.1 MANE BI network

We developed 29 LWBI chronologies across the MANE region, all of which were used as predictors in the $T_{Mar-Sep}$ reconstruction (Fig. 1AB; Table S2). Of the 29 records, 28 derive from *T. canadensis* and one from *P. rubens*. The relationships between LWBI predictor chronologies and the target $T_{Mar-Sep}$ predictand data varies in the reconstruction model from $r=0.28$ (Salt Springs State Park, PA) to $r=0.68$ (Alander Mountain, MA) over the 1901−1976 period ($p<0.10$). The 28 chronologies included in the reconstruction did not vary substantially in elevation (Harley et al. 2021), but they did vary by latitude. However, results show a non-linear relationship found between latitude and each site PC_1 loading (Fig. S2). We attribute this non-linear relationship to microclimate site characteristics of *T. canadensis* and the species' propensity to inhabit cove-like, cold air traps across the landscape (Cook and Cole 1991). As the LWBI network across this region expands to include more *T. canadensis* chronologies as well as more high-elevation species, such as *P. rubens*, perhaps significant relationships between site latitude and/or elevation will be more clearly elucidated.

Further related to our analysis of site characteristics that might influence signal detection, we observed negative impacts of disturbance from hemlock woolly adelgid (HWA; *Adelges tsugae* Annand) at several sites across the MANE network. We experienced a failed attempt in May 2021 to update the Sweet Root Natural Area site in Pennsylvania, where we observed complete HWA-caused mortality of *T. canadensis* individuals that were originally cored at the site by Cook and Cole (1991) *ca.* 1982. The other site from which we observed marked impacts from HWA was Alander Mountain, Massachusetts. After coring this site in summer 2022 and developing the LWBI chronology, we noticed a severe impact in ring widths starting during the period 2006−2008 that was characterized by [1] narrow total and latewood widths that were also [2] light in color (*e.g.* thin tracheid walls throughout). Growth rings with such characteristics can bias BI data because of the absence of lignin caused by the disturbance agent, which in turn can weaken the climate signal fidelity (Seftigen et al. 2020). Given this narrow ring bias is most likely attributed to the negative impacts of HWA at the site, we truncated this record to the year 2005, before which HWA impacted trees.

3.2 Model calibration and verification

The common period model spanned the period 1901−1976 over which the first PC (distilled from 29 sites and 983 tree cores) explains 62% of $T_{Mar-Sep}$ variance (Table S3; Fig. 3B). The reconstruction comprised 16 backward nests extending to the year 1461. We also performed eight forward nests from 1977 to 2021. Going backward in time, the model nests remained robust, explaining over 40% of the instrumental variance with strong and positive RE (0.28-0.67) and CE (0.26-0.68) values until *ca.* 1550. The reconstruction remains valid with positive RE and CE statistics back to 1461 (Fig. 3D), however, as the number of tree-ring chronologies
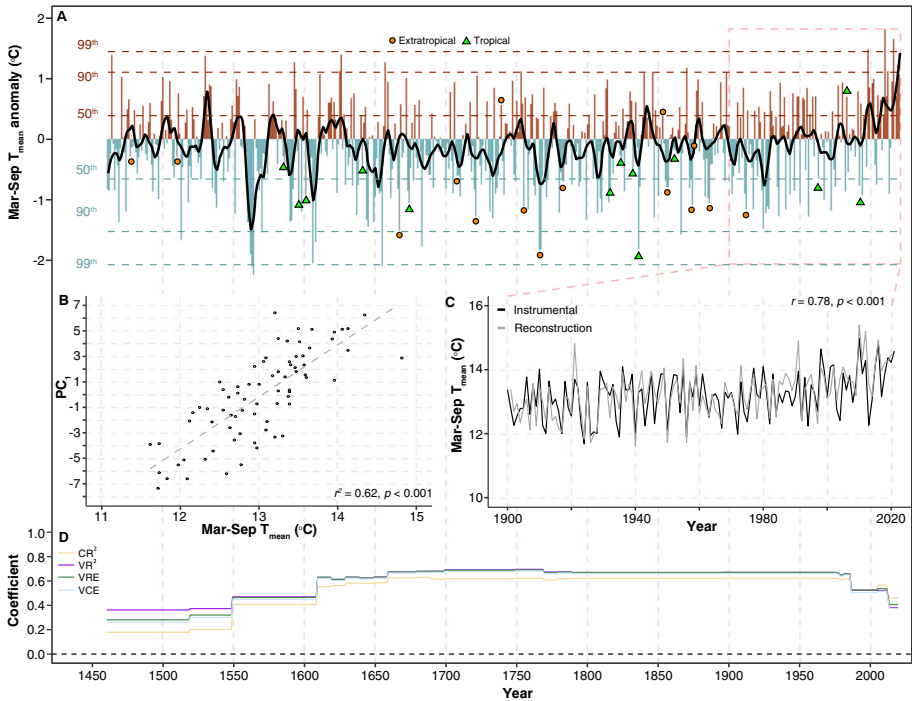
Fig. 3 MANE summer temperatures since 1998 CE are unprecedented over the past ca. 561 years (A) $T_{Mar-Sep}$ reconstruction shown as anomalies (rel. to 1951-1980 mean) from $1461-2021$ CE (red and blue bars) smoothed with a 20 y low pass filter (black) and 50, 90, and 99th percentiles (dashed lines). Orange circles (green triangles) are extratropical (tropical) volcanic eruption years, with tropical years adjusted by +1 year to match the cooling response. (B) Scatter plot $T_{Mar-Sep}$ °C values versus PC_1 of the MANE BI network during the period $1901-1976$. (C) Line graph showing agreement of the reconstruction (gray) and $T_{Mar-Sep}$ (black) during the period $1901-2021$. (D) Reconstruction validation statistics for each nest showing calibration period R_2 (CR^2; yellow), verification period R_2 (VR^2; purple), verification period reduction of error (VRE; green), and verification period coefficient of efficiency (VCE; blue)

drops to $n=2$ at 1549, the calibration and verification period R^2 values decline to 0.20 and 0.37, respectively, weakening model estimates. Although the two nests before 1550 passed validation tests, the models explained 20% and 18% of the instrumental variance, hence values before 1550 should be interpreted with caution. The ability to place the current warming trend in a long-term context was a primary objective of this study. The explanatory power of forward model nests remained high until 2020 (46%) as a result of the abundance of updated tree-ring chronologies included in this study. The final temperature reconstruction benefited from these recollections and updates to *T. canadensis* chronologies that were originally sampled throughout the region in the late 1970s and through the 1980s and presented in Cook and Cole (1991).

3.3 MANE summer temperatures since 1461 CE

We provide a 561-year ($1461-2021$ CE) reconstruction of warm season $T_{Mar-Sep}$ for MANE (Fig. 3A). The warmest reconstructed year is 2010 at +1.8 °C above the $1951-1980$ mean, exceeding the 99th percentile. This finding is corroborated by the instrumental data, with 2010 having the warmest single-year summer since 1901 (+2.27 °C). The small discrepancy in

anomalies calculated for the reconstruction versus the instrumental data highlights the fact that our reconstruction should be considered a conservative estimate of temperature due to general, yet slight, model underprediction (*e.g.* reconstructed warm (cool) years were most likely warmer (cooler) than estimated) (Esper et al. 2005) (Fig. S1A-D). Assessment of model fit reveals an underestimation of target high-frequency variance particularly over the most recent *ca.* 20 years (Figs. 3C; S3). This was expected given the reduction in predictor chronologies in the most recent forward nests. Given the propensity of MANE reconstruction model over- and under-predictions, bias-correction Robeson et al. 2020 provided more accurate estimations of temperature for the reconstruction model (Fig. S1B,D), and subsequently for the full reconstruction (Fig. S1A).

Placing recent conditions within the context of the past 561 years, summer temperatures in 12 of the top 20 warmest single-year anomalies have occurred since the turn of the 21st century (2002, 2005, 2010−2012, 2015−2021) (Fig. 4). The warmest multi-year events since 1461 were 2009−2012 ($\overline{x}$ anomaly +1.10 °C) and 2015−2021 ($\overline{x}$ +1.09 °C). Similar to the 21st century, the 16th century and early 17th centuries contain three of the most severe warm events, with 1593−1594 (+1.13 °C) being a short but intense positive departure, and 1575−1580 (+0.58 °C) and 1528−1534 (+0.78 °C) expressed as less intense but more pro-
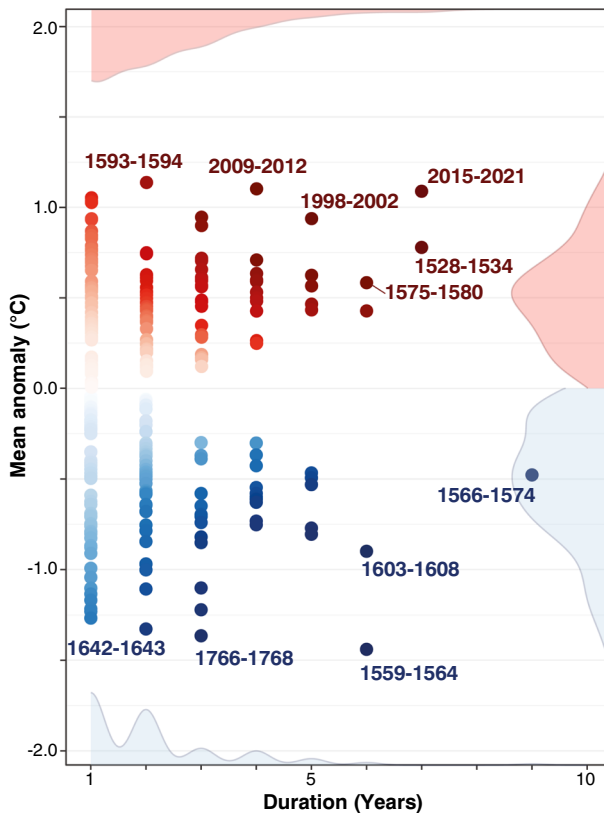

Fig. 4 **MANE summer temperatures in 12 of the top 20 warmest single-year anomalies have occurred since the turn of the 21st century.** Bivariate characterization of multi-year warm (red) and cool (blue) events in the MANE T$_{Mar-Sep}$ reconstruction colored by magnitude (intensity/duration). Intensity (y-axis) and duration (x-axis) density plots shown on each margin

longed departures. Unlike the 21st century, the 16th−early 17th century also includes three of the most pronounced cool summer events across the region (-0.45 °C from 1566−1574, -0.87 °C from 1603−1608, and -1.4 °C from 1559−1564).

Our LWBI-based T$_{Mar-Sep}$ reconstruction shows multi-decadal agreement ($p < 0.05$) with other historical temperature records (proxy-based and instrumental) across various spatial scales (Fig. 5). In particular, 30-year temperature trends in MANE are significantly and positively correlated with the New Haven instrumental record, as well as temperature variability across the Southeast US (King et al. In Press) and eastern Canada (Wang et al. 2022). Interestingly, we note significant, negative associations between MANE and temperature reconstructions from western North America (*e.g.* Yellowstone (Heeter et al. 2021), Pacific Northwest (Heeter et al. 2023), Interior British Columbia (Luckman and Wilson 2005), and southern Yukon (Wilson et al. 2019) (Fig. 5). The atmospheric drivers of midlatitude climate dipoles are becoming increasingly important to understand given their broad effect on ecological processes. Driven by Rossby waves associated with convection from the Madden-Julian oscillation and East Asian monsoon, the North American Dipole (NAD) is characterized
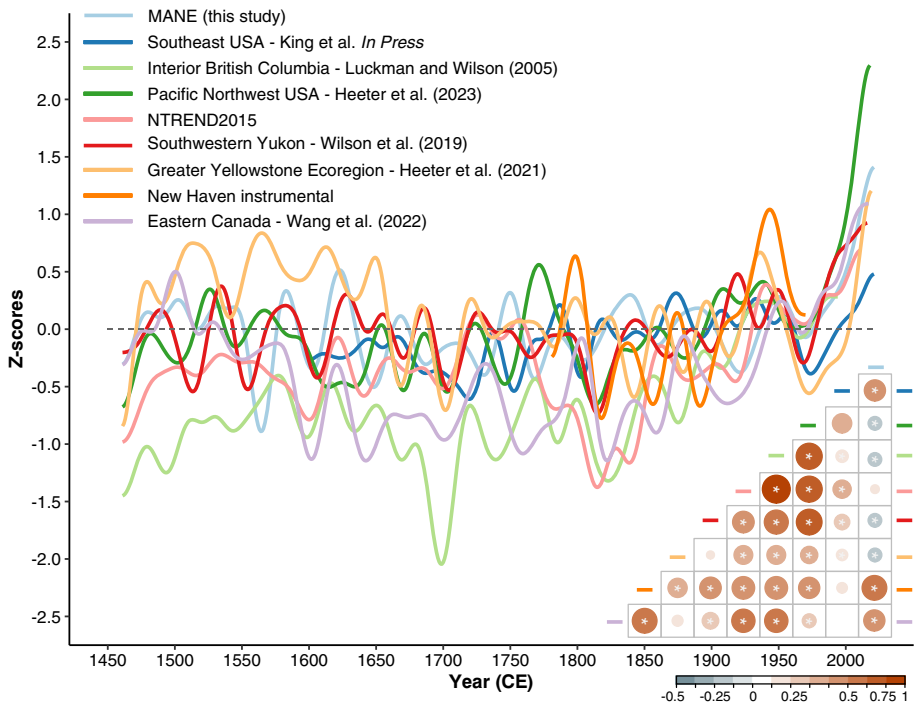

Fig. 5 Comparison of MANE T$_{Mar-Sep}$ with other historical records of summer temperatures. Smoothed (30-year low-pass filter) versions of each record are plotted as z-scores relative to the mean and standard deviation over the period 1951-1980 CE. Also plotted is a Pearson's correlation matrix between each time series calculated over the common period of all reconstructions. Asterisks indicate significance at the $p < 0.05$ level. Lines plotted are: MANE Mar-Sep T$_{mean}$ (this study; light blue); Southeast USA Aug-Sep T$_{max}$ King et al. (In Press)(dark blue); Interior British Columbia "Icefield" May-Aug T$_{max}$ (Luckman and Wilson 2005)(light green); Pacific Northwest USA Jun-Aug T$_{mean}$(Heeter et al. 2023)(dark green); NTREND2015 May-Aug T$_{mean}$(Wilson et al. 2016)(pink); Greater Yellowstone region Aug T$_{max}$(Heeter et al. 2021)(light orange); instrumental Mar-Sep T$_{mean}$ from New Haven, Connecticut, USA (dark orange); Eastern Canada/Northeast North America (NENA) May-Aug T$_{mean}$(Wang et al. 2022)(purple); and Southwestern Yukon May-Aug T$_{max}$(Wilson et al. 2019)(red)

by an east-west dipole pattern (*e.g* with centers over the Northeast/Upper Midwest US and Pacific Northwest) in 500-hpa geopotential height, temperature, and precipitation during the boreal summer (JJA) (Bai et al. 2023). The recently-developed, long-term summer temperature records across eastern Canada (Wang et al. 2022), MANE, and the southeast US (King et al. In Press) now make it possible to investigate the consistency in the NAD for the past couple hundred years and across space.

Pearl et al. (2017) used *C. thyoides* growth rings to reconstruct mean Jan-Aug temperatures from 1872−2014. Although the pre-instrumental period of overlap between the two records is short, both records demonstrate a cooler-than-average 1870s followed by average temperature conditions before the cooling of the turn of the 20th century. Further, we find significant and positive multi-decadal coherence ($r=0.40$, $p<0.001$) with a maximum latewood density (MXD)-based reconstruction of mean May-Aug temperatures from northeastern North America (NENA) from 1461−2017—the common period of overlap between the two records (Wang et al. 2022) (Fig. 3D). Although the length of our record precludes us from characterizing the historical context of modern warming as compared to the Medieval Climate Anomaly (MCA; *ca.* 950−1250 CE), we do capture the cooler-than-average summers of the Little Ice Age (LIA) during the 16th through 19th centuries. Most notable during this period are the aforementioned cool events of the late 16th−early 17th century, as well as the *ca.* 100-year period of cooler-than-average summers from 1640s−1740s, which is marked by reduced variability in the record. This period of cool summers is contemporary with the 16th century Megadrought that, although less severe in the eastern US compared to the western US, is still discernible in the North American Drought Atlas (Cook et al. 1999). One noteworthy distinction between the MANE and NENA reconstructions during the LIA is comparatively lower average summer temperatures expressed by NENA. We attribute this difference to [1] the higher-latitude and inland locations of predictor sites in Wang et al. (2022) compared to this study, and [2] the varied proxy indicators between the two studies; NENA is a record derived from MXD and we exclusively use BI.

3.4 Volcanic forcing of MANE temperatures

One of the primary contributors to anomalously cool summer conditions is volcanic forcing (Self et al. 1981; Cole-Dai 2010; Robock 2000; Esper et al. 2013, 2017; Büntgen et al. 2020). The influence of large-scale volcanic eruptions on summer temperatures is also apparent across eastern Canada (Gennaretti et al. 2014; Wang et al. 2022) as well as over adjacent lower latitudes of MANE. Cool summers across MANE since 1461 were frequently related to volcanic eruptions. Using a bootstrapped SEA, we find significant ($p<0.05$) departures in MANE temperatures were associated with both tropical ($n=13$) and extratropical ($n=15$) volcanic events, with a demonstrated lag effect depending upon spatial location of eruption (Fig. 6A-D). Tropical eruptions yielded a consistent +1 year lag effect on MANE $T_{Mar-Sep}$, while eruptions from extratropical locations had an effect on $T_{Mar-Sep}$ only during the year of the event, a similar result demonstrated by the NENA reconstruction from eastern Canada (Wang et al. 2022). We attribute this difference in lagged effect on MANE $T_{Mar-Sep}$ to the fact that previous research has shown that tropical volcanoes often inject aerosols into the lower stratosphere that migrate poleward and reside for 1−3 years (Schneider et al. 2009; Toohey et al. 2019; Burke et al. 2023). Extratropical eruptions, however, produce aerosols mainly limited to the region 30-90 °N and have shorter atmospheric residence times (Oman et al. 2005; Kravitz and Robock 2011). The expansion of high-resolution, temperature-sensitive proxies across the Northern Hemipshere (Kaczka and Wilson 2021), particularly across east-
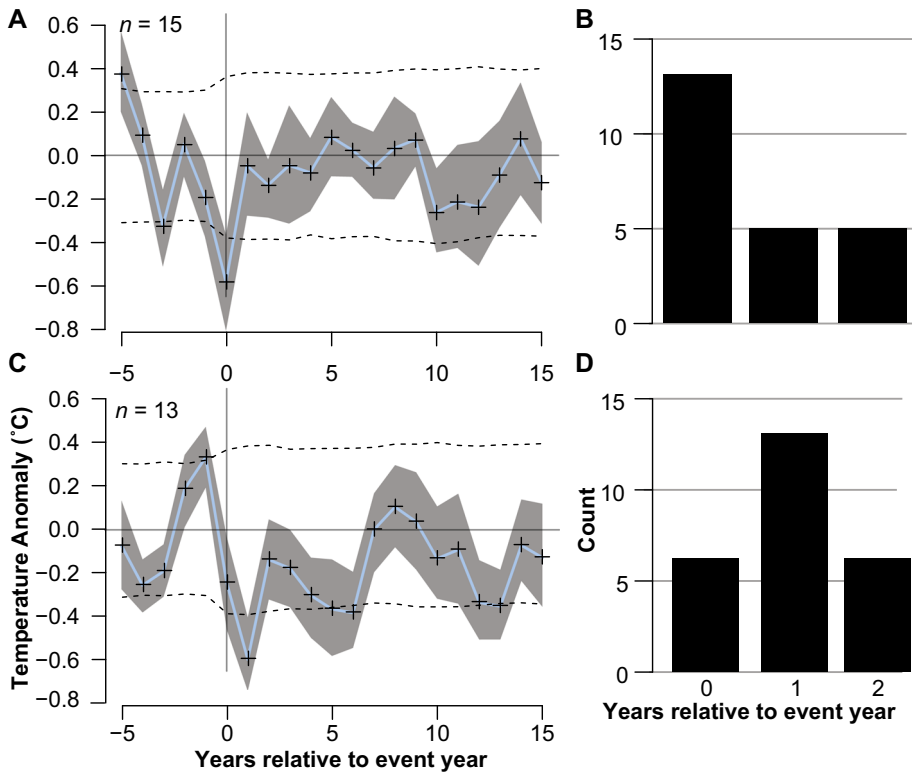
Fig. 6 Global volcanic eruption impacts on MANE summer temperatures. Superposed epoch analysis (SEA) between the MANE $T_{Mar-Sep}$ reconstruction and the largest volcanic extratropical (A; $n=15$) and tropical (C; $n=13$) eruptions from $1461-1900$ CE. Also shown is the timing of cooling minima during the period 2 years following the 0-year event for (B) extratropical and (D) tropical eruptions. SEA displays the temperature anomalies for the period 5 years before and 15 years after each eruption. Uncertainty envelop (gray) is constructed using random bootstrapping (Rao et al. 2019) and horizontal dashed lines represent $\alpha=0.05$. Eruptions are based on ice core sulfate records from the Global Volcanism Program Volcanoes of the World database (v. 5.1.7) and listed in Toohey and Sigl (2017) with additional large, instrumental-period eruptions of 1912 (Novarupta), Agung (1963), 1982 (El Chicon), and 1991 (Pinatubo) included. Eruptions used for analyses are listed in Table S1

ern North America, presents an opportunity to disentangle the effects of eruption origin (tropical vs extra-tropical) and timing on summer cooling. Yet, as we learned from Edwards et al. (2021), developing QWA metrics for these regions will be necessary to more accurately constrain differences in the timing response to volcanic forcing.

Of the 28 volcanic events we consider, summer temperatures were below the 1951-1980 mean in response to 25 of those eruptions (90%). MANE $T_{Mar-Sep}$ fails to capture a response from 1 tropical (El Chichon in 1982) and 2 extratropical eruptions, both on Japan (Shikotsu (Tarumai) and Toya (O-Usu) in 1667 and 1853, respectively) (Table S1). We were not surprised by the lack of summer cooling shown in the MANE $T_{Mar-Sep}$ record in $1982-1983$ due to the fact that tropospheric temperatures across the Northern Hemisphere warmed following the eruption of El Chichon, which has been attributed to the strong El Nino event in $1982-1983$ that yielded anomalously warm SSTs in the eastern equatorial Pacific Ocean (Angell and Korshover 1984).

Broader-scale T$_{mean}$ records across the Northern Hemisphere tend to contain a more robust response to volcanic forcing, where most of the coldest years are associated with volcanic eruptions and the response is prolonged by *ca.* 3-5 years (e.g. Anchukaitis et al. 2012; D'Arrigo et al. 2013; Anchukaitis et al. 2017; Wilson et al. 2017. Yet, in the more regional-scale, lower-latitude MANE record, not all of the single- and multi-year cool events identified via bivariate analysis seem to be volcanically forced (Fig. 3A;4. Of the top 25 coolest summer temperature events identified, 8 were linked with either a tropical or extratropical eruption (ranked): 1766-1768 (Hekla (Bjallagigar); $\overline{x}$ anomaly -1.84 °C), 1835-1837 (Cosiguina; -1.81°C), 1642-1643 (Parker; -1.3°C), 1755-1756 (Katla; -1.11°C), 1510-1513 (Hekla; -0.97°C), 1603-1608 (Huaynaputina; -0.92°C), 1885-1886 (Krakatau and/or Okataina (Tarawera); -0.88°C), and 1991-1992 (Pinatubo; -0.83°C). We find that more of the identified cool events in MANE summer temperatures (Fig. 4), in particular the prolonged and severe cooling event of 1559−1574 CE, were likely unforced by volcanism and either related to atmospheric circulation or stochastic variability (Anchukaitis et al. 2017, 2019; Anchukaitis and Smerdon 2022; Marshall et al. 2021). Acting as the geographically closest record to MANE for comparison, temperature departures in the higher-latitude, MXD-based reconstruction from Wang et al. (2022) are more-consistently volcanically forced.

The most severe summer cooling event in the Wang et al. (2022) NENA reconstruction occurred in 1816 in response to the eruption of Mount Tambora in April 1815, marked as a -4.53 °C departure from the 1905−2006 CE mean. Pearl et al. (2020b) built upon their earlier study and produced a gridded field reconstruction of Jan-Aug temperatures since the early 1800s for the Northeast US. In response to the eruption of Tambora, they highlight widespread cooling of 1−3 °C across much of the region that lasted for two years (1816−1817) as one of the coldest periods in the reconstruction. To people in Europe and the Northeast US, the summer of 1816 came to be known as 'the year without a summer' due to the abnormally-low daily minimum temperatures from late spring through early fall (Stothers 1984). Mean Mar-Sep temperature anomalies from the New Haven (CT) instrumental record (rel. to the 1781-1970 mean) fell -1.1, -2.9, -1.6, and -1.2 °C in 1815−1818, respectively). Although, as noted by Angell and Korshover (1985) and Stothers (1984), growing season temperatures were already on the decline for several years before 1815, most likely due to the eruption of 1809 (unidentified) (Timmreck et al. 2021). We also see this cooling trend prior to Tambora captured in the MANE record, with temperature departures (°C) in 1809 (1810) of -1.30 (-1.64), as well as across the Pacific Northwest US of -0.51 (-1.68) (Appleton and George 2018; Heeter et al. 2023), Interior British Columbia of -0.75 (-1.99) (Luckman and Wilson 2005), Southwestern Yukon of -0.50 (-2.42) (Wilson et al. 2019), Greater Yellowstone Ecoregion of -1.21 (-1.69), and a slight response across the Southeast US of +1.06 (-0.36). Leland et al. (2023) reports that across the broader northwestern North America, cooling in response to the 1809 eruption was centered around the Gulf of Alaska and southern Yukon, but diminished with distance from this region. Interestingly, the NENA record does not capture the eruption of 1809 across eastern Canada, with temperature anomalies of +0.37 (+0.42). The expansion of BI and MXD records across eastern North America and the Midwest US will make a spatiotemporal assessment of the 1809 eruption possible across this region (*c.f.* Leland et al. (2023)

We note a response in summer temperatures across MANE to the 1815 eruption with a departure from mean conditions starting in 1815 (-1.05 °C) and persisting until 1818 (-0.80 °C in 1816, -0.30 °C in 1817, and -0.57 °C in 1818), with an average temperature anomaly of -0.68 °C during this 4-year period. Although we observe a slight cooling event in response to the Tambora eruption, our reconstruction suggests that summer temperature departures were not as extreme across MANE compared to the higher latitude Wang et al. (2022) study or the

Pearl et al. (2020b) study. Yet, differences in seasonality (*e.g.* Mar-May for NENA and Jan-Aug for Pearl et al. (2020b) versus Mar-Sep for MANE) and the ability of various proxies to precisely capture the imprint of volcanic cooling (*e.g.* MXD versus BI; Edwards et al. 2021) might explain this disparity. We did notice, however, that one of the primary reasons for the subdued response in the MANE $T_{Mar-Sep}$ record to the Tambora eruption is likely due to our inclusion of predictor BI chronologies from locations outside of the Northeast US, as the most extreme temperature departures from this event were likely centered across New England and diminished with distance from this region (Hoyt 1958; Stothers 1984). As such, we note that the site-specific response to Tambora varied across the MANE network. For example, our BI sites from Maryland and Pennsylvania demonstrate positive temperature anomalies between +0.20 and +0.50 °C during the 1815−1818 period. However, sites from the northern portion of the network (*e.g.* Connecticut, New York, New Hampshire, Vermont, and Maine) show strong summer temperature departures of <-1.0 °C, which matches the spatial extent of the summer cooling across the Northeast US reconstructed by Pearl et al. (2020b).

3.5 Ocean/atmosphere drivers of MANE temperatures

Our analysis shows a significant ($r>0.50$, $p<0.05$) spatial relationship between the MANE reconstruction and sea surface temperatures (SST) in the adjacent, near-shore Atlantic Ocean centered around the Gulf of Maine (Fig. 7D). Pearl et al. (2017) and Pearl et al. (2020b) demonstrated the same significant and positive relationship between Northeast US land and SSTs, although they report a broader spatial connection over much of the North Atlantic Ocean. Most MANE predictors are positioned considerably inland and at higher elevations compared to the coastal *C. thyoides* chronologies included in previous Northeast US temperature reconstructions (Pearl et al. 2017, 2020b), most likely explaining the differences in the spatial imprinting of SSTs to each record. A multi-proxy network that combines the strong temperature proxies of *C. thyoides* (Pearl et al. 2020b) with the LWBI-derived MANE network as well as other tree-ring width chronologies from the region shown to demonstrate a sensitivity to growing season temperatures (Patterson et al. 2016) would produce a potentially more robust pool of candidate predictors across a region known for diverse and complex relationships between tree species and temperature Pederson et al. (2004); Alexander et al. (2019); Maxwell et al. (2020).

Analyses from Belmecheri et al. (2017) on the relationships between seasonal 300-hpa positions of the tropospheric Northern Hemisphere polar jet stream (NHJ), precipitation, and temperature since 1930 CE across North America note that the position of the NHJ during summer displays a dipole pattern characterized by positive temperature anomalies across the MANE region associated with higher latitude NHJ trajectories. In support of a possible connection between MANE summer temperatures and the NHJ, we find that increased 300-hpa meridional (zonal) wind stress produces decreased (increased) summer temperatures across MANE (Fig. 7A,B). The negative correlation (r range -0.20 to -0.50, $p<0.05$) between meridional wind stress and summer temperatures over MANE matches the "JA-6" (JA=July-August or summer season; Belmecheri et al. 2017) longitudinal position pattern of the NHJ, whereby a meridional undulation funnels high-latitude air towards the lower latitude MANE region. Conversely, increased zonal wind stress north of ∼55 °N, as shown in Fig. 7B, results in warmer summer temperatures, most likely due to the facilitation of higher pressure over the region as well as over the British Isles (Fig. 7C), a pattern also highlighted by Belmecheri et al. (2017). However, fully disentangling the long-term influences of the NHJ on summer
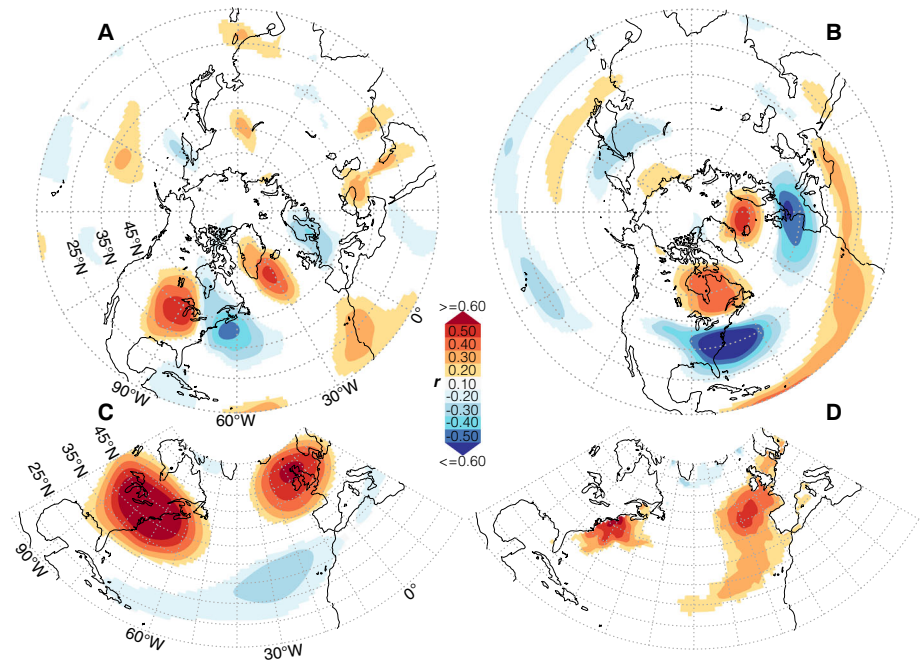
Fig. 7 Dynamical climate characteristics of the MANE T$_{Mar-Sep}$ reconstruction corroborate linkages with the NHJ. Spatial correlation (1*st*-differenced) between the MANE T$_{Mar-Sep}$ reconstruction versus 300-hpa meridional (A) and zonal (B) wind stress (20CRv3) during the period 1901−2021, (C) 500-hpa geopotential height (20CRv3; 1901−2021), and (D) sea surface temperatures (HadISST) 1901−2021

temperatures across MANE with our dataset is precluded by the lack of temperature-sensitive tree-ring records located in key regions with demonstrated NHJ-temperature relationships, such as central North America.

Trouet et al. (2018) use temperature-sensitive tree-ring records from Europe to reconstruct interannual variability in the latitudinal position of the August NAJ back to 1725 CE. The spatial footprint of their reconstruction model shows strong relationships between the Aug NHJ position and instrumental summertime air temperatures over central North America (centered over the Great Lakes region as described in Figure 1A,B from Trouet et al. 2018) during the period 1920−2012. Despite not including any sites from outside the MANE region, our reconstruction demonstrates strong spatial correlations over the Great Lakes, broader Upper Midwest US, and central Canada ($r \geq 0.60$, $p < 0.001$; Fig. S4), which we note as a direction in which to expand this research by developing temperature-sensitive proxies (*e.g.* LWBI, MXD, QWA) over Central North America to combine with existing records across MANE, the Pacific Northwest (Heeter et al. 2023), and western Europe (Trouet et al. 2018) to increase our understanding of continental-scale, long-term linkages between summer temperature anomalies and NHJ dynamics (Wise and Dannenberg 2014; Trouet et al. 2018; Osman et al. 2021).

4 Conclusions

Assessment of an improved network of BI tree-ring chronologies across the MANE region reveals an unprecedented warming trend over the past 30 years including 12 of the top 20

warmest summers since 1461 CE. Temperature variability across MANE is linked with large-scale extratropical and tropical volcanic eruptions, as well as regional, coastal sea-surface temperatures, 500-hpa geopotential height, and 300-hpa meridional and zonal wind vectors. The expansion of the LWBI-derived MANE network to the west (central North America) and southeast US and the combination with existing temperature-sensitive proxies across North America (Heeter et al. 2020, 2021; Wilson et al. 2019; Wiles et al. 2019; Edwards et al. 2021; Trinies et al. 2022; Gennaretti et al. 2014; Wang et al. 2022; Heeter et al. 2019) will be critical for a more comprehensive understanding of spatiotemporal dynamics of temperature variability over the last millennium (*e.g.* values, trends, compound climate extremes). This would foster our insights into the direct impact of long-term NHJ dynamics on continental-scale summer temperatures (Coumou and Rahmstorf 2012; Williams and Joshi 2013; Chen et al. 2014). Such improvements to the MANE network, however, are challenging as many viable species for BI in the eastern US (Harley et al. 2021) are already included in the MANE network. This could be overcome by developing BI chronologies from *P. rubens* that would offer additional sites across the species range and at higher elevations, which might lead to more comprehensive estimations of temperatures. Moreover, the temporal extension of BI chronologies can be achieved by successfully including subfossil and historical material retrieved across the Mid-Atlantic and Northeast USA, which dates as far back as at least the past several thousand years (Pearl et al. 2020a). We, therefore, propose to extend the MANE network back in time through [1] the application of QWA or BI to existing subfossil *C. thyoides* material (Pearl et al. 2020a) using resin-extraction processes outlined in Heeter et al. (2022) and [2] the acquisition of old-growth *T. canadensis* and *P. rubens* used in historical structures or found at the bottom of cold lakes (Lorentzen 2023; Krusic et al. 2015).

Author Contributions GLH, JTM, KEK, SAR, and ERC conceived the paper and designed analyses. GLH, JTM, KEK, SAR, CH, RSM, FR, and JE collected the data. ERC, RSM, FR, and JE contributed data and analysis tools. GLH, JTM, KEK, SAR, CH, TFS, EVB, KEB, NK, BL, and RDT performed the analyses. GLH, JTM, KEK, SAR, ERC, CH, RSM, FR, JE, TFA, EVB, KEB, NK, BL, and RDT wrote the paper.

Data Availability All tree-ring measurements and reconstruction products are available through the U.S. National Oceanic and Atmospheric Administration World Data Service for Paleoclimatology International Tree Ring Databank (https://ncei.noaa.gov/products/paleoclimatology/tree499_ring).

Declarations

Ethical Standards The authors comply with all ethical standards. No human or animal subjects were involved with this research.

Competing Interests The authors have no relevant financial or non-financial interests to disclose.

References

Akaike H (1974) A new look at the statistical model identification. In: Selected papers of Hirotugu Akaike. Springer, pp 215–222

Alexander MR, Pearl JK, Bishop DA, Cook ER, Anchukaitis KJ, Pederson N (2019) The potential to strengthen temperature reconstructions in ecoregions with limited tree line using a multispecies approach. Quatern Res 92(2):583–597

Anchukaitis KJ, Smerdon JE (2022) Progress and uncertainties in global and hemispheric temperature reconstructions of the common era. Quat Sci Rev 286:107537

Anchukaitis KJ, Breitenmoser P, Briffa KR, Buchwal A, Büntgen U, Cook ER, D'arrigo RD, Esper J, Evans MN, Frank D et al (2012) Tree rings and volcanic cooling. Nat Geosci 5(12):836–837

Anchukaitis KJ, Wilson R, Briffa KR, Büntgen U, Cook ER, D'Arrigo R, Davi N, Esper J, Frank D, Gunnarson BE et al (2017) Last millennium northern hemisphere summer temperatures from tree rings: part ii, spatially resolved reconstructions. Quatern Sci Rev 163:1–22

Anchukaitis KJ, Cook ER, Cook BI, Pearl J, D'Arrigo R, Wilson R (2019) Coupled modes of north atlantic ocean-atmosphere variability and the onset of the little ice age. Geophys Res Lett 46(21):12417–12426

Angell JK, Korshover J (1985) Surface temperature changes following the six major volcanic episodes between 1780 and 1980. J Clim Appl Meteor, pp 937–951

Angell J, Korshover J (1984) Comparison of tropospheric temperatures following agung and el chichón volcanic eruptions. Mon Weather Rev 112(7):1457–1463

Appleton SN, George SS (2018) High-elevation mountain hemlock growth as a surrogate for cool-season precipitation in crater lake national park, usa. Dendrochronologia 52:20–28

Bai H, Strong C, Zuckerberg B (2023) Drivers of an ecologically relevant summernorth american dipole. J Clim 36(8):2387–2399

Belmecheri S, Babst F, Hudson AR, Betancourt J, Trouet V (2017) Northern hemisphere jet stream position indices as diagnostic tools for climate and ecosystem dynamics. Earth Interact 21(8):1–23

Belmecheri S, Maxwell RS, Taylor AH, Davis KJ, Guerrieri R, Moore DJ, Rayback SA (2021) Precipitation alters the co2 effect on water-use efficiency of temperate forests. Glob Change Biol 27(8):1560–1571

Bunn AG (2008) A dendrochronology program library in r (dplr). Dendrochronologia 26(2):115–124

Bunn AG (2010) Statistical and visual crossdating in r using the dplr library. Dendrochronologia 28(4):251–258

Büntgen U, Arseneault D, Boucher E, Churakova OV, Gennaretti F, Crivellaro A, Hughes MK, Kirdyanov AV, Klippel L, Krusic PJ et al (2020) Prominent role of volcanism in common era climate variability and human history. Dendrochronologia 64:125757

Burke A, Innes HM, Crick L, Anchukaitis KJ, Byrne MP, Hutchison W, McConnell JR, Moore KA, Rae JW, Sigl M et al (2023) High sensitivity of summer temper atures to stratospheric sulfur loading from volcanoes in the northern hemisphere. Proc Natl Acad Sci 120(47):e2221810120

Cao X, Hu H, Kao Pk, Buckley BM, Dong Z, Chen X, Zhou F, Fang K (2022) Improved spring temperature reconstruction using earlywood blue intensity in southeastern china. Int J Climatol 42(12):6204–6220

Chen K, Gawarkiewicz GG, Lentz SJ, Bane JM (2014) Diagnosing the warming of the northeastern us coastal ocean in 2012: a linkage between the atmospheric jet stream variability and ocean response. J Geophys Res: Oceans 119(1):218–227

Cole-Dai J (2010) Volcanoes and climate. Wiley Interdisciplinary Reviews: Climate Change 1(6):824–839
Compo GP, Whitaker JS, Sardeshmukh PD, Matsui N, Allan RJ, Yin X, Gleason BE, Vose RS, Rutledge G, Bessemoulin P et al (2011) The twentieth century reanalysis project. Q J R Meteorol Soc 137(654):1–28
Conkey LE (1986) Red spruce tree-ring widths and densities in eastern North America as indicators of past climate. Quatern Res 26(2):232–243
Cook ER, Cole J (1991) On predicting the response of forests in Eastern North America to future climatic change 19:271–282
Cook ER, Peters K (1981) The smoothing spline: a new approach to standardizing forest interior tree-ring width series for dendroclimatic studies. Tree-Ring Bulletin 41:45–53
Cook ER, Peters K (1997) Calculating unbiased tree-ring indices for the study of climatic and environmental change. The Holocene 7(3):361–370
Cook ER, Meko DM, Stahle DW, Cleaveland MK (1999) Drought reconstructions for the continental united states. J Clim 12(4):1145–1162
Cook ER, Woodhouse CA, Eakin CM, Meko DM, Stahle DW (2004) Long-term aridity changes in the western united states. Science 306(5698):1015–1018
Cook ER, Seager R, Cane MA, Stahle DW (2007) North American drought: re-constructions, causes, and consequences. Earth-Sci Rev 81(1–2):93–134
Coumou D, Rahmstorf S (2012) A decade of weather extremes. Nat Clim Chang 2(7):491–496
D'Arrigo R, Wilson R, Anchukaitis KJ (2013) Volcanic cooling signal in tree ring temperature records for the past millennium. J Geophys Res: Atmospheres 118(16):9000–9010
Edwards J, Anchukaitis KJ, Zambri B, Andreu-Hayles L, Oelkers R, D'Arrigo R, von Arx G (2021) Intra-annual climate anomalies in northwestern north america following the 1783-1784 ce laki eruption. J Geophys Res: Atmospheres, p e2020JD033544
Esper J, Cook ER, Schweingruber FH (2002) Low-frequency signals in long tree-ring chronologies for reconstructing past temperature variability. Science 295(5563):2250–2253
Esper J, Schneider L, Krusic PJ, Luterbacher J, Büntgen U, Timonen M, Sirocko F, Zorita E (2013) European summer temperature response to annually dated volcanic eruptions over the past nine centuries. Bull Volcanol 75:1–14
Esper J, Büntgen U, Hartl-Meier C, Oppenheimer C, Schneider L (2017) Northern hemisphere temperature anomalies during the 1450s period of ambiguous volcanic forcing. Bull Volcanol 79:1–9
Esper J, Frank DC, Wilson RJS, Briffa KR (2005) Effect of scaling and regression on reconstructed temperature amplitude for the past millennium. Geophys Res Lett 32(7). https://doi.org/10.1029/2004gl021236
Foster JR, D'Amato AW (2015) Montane forest ecotones moved downslope in northeastern usa in spite of warming between 1984 and 2011. Glob Change Biol 21(12):4497–4507
Frank D, Esper J, Cook ER (2007) Adjustment for proxy number and coherence in a large-scale temperature reconstruction. Geophys Res Lett 34(16)
Fritts H (1976) Tree rings and climate. Elsevier
Gennaretti F, Arseneault D, Nicault A, Perreault L, Bégin Y (2014) Volcano-induced regime shifts in millennial tree-ring chronologies from northeastern north america. Proc Natl Acad Sci 111(28):10077–10082
González J, Valdés JB (2003) Bivariate drought recurrence analysis using tree ring reconstructions. J Hydrol Eng 8(5):247–258
Guttman L (1954) Some necessary conditions for common-factor analysis. Psychometrika 19(2):149–161
Harley GL, Heeter KJ, Maxwell JT, Rayback SA, Maxwell RS, Reinemann TE, Taylor H, A, (2021) Towards broad-scale temperature reconstructions for eastern north america using blue light intensity from tree rings. Int J Climatol 41:E3142–E3159
Harris I, Osborn TJ, Jones P, Lister D (2020) Version 4 of the cru ts monthly high-resolution gridded multivariate climate dataset. Scientific data 7(1):109
Heeter KJ, Harley GL, Maxwell JT, McGee JH, Matheus TJ (2020) Late summer temperature variability for the Southern Rocky Mountains (USA) since 1735 CE: applying blue light intensity to low-latitude Picea engelmannii Parry ex Engelm. Climatic Change, pp 1–24
Heeter KJ, Harley GL, Van De Gevel SL, White PB (2019) Blue intensity as a temperature proxy in the eastern united states: a pilot study from a southern disjunct population of picea rubens (sarg.). Dendrochronologia 55:105–109
Heeter KJ, Rochner ML, Harley GL (2021) Summer air temperature for the Greater Yellowstone Ecoregion (770–2019 CE) over 1,250 years. Geophys Res Lett 48(7):e2020GL092269
Heeter KJ, King DJ, Harley GL, Kaczka RJ (2022) Video tutorial: measuring blue intensity with the coorecorder software application. Dendrochronologia 76:125999
Heeter KJ, Harley GL, Abatzoglou JT, Anchukaitis KJ, Cook ER, Coulthard BL, Dye LA, Homfeld IK (2023) Unprecedented 21st century heat across the pacific northwest of north america. npj Clim Atmos Sci 6(1):5

Hopton HM, Pederson N (2005) Climate sensitivity of atlantic white cedar at its northern range limit. In: Atlantic White Cedar: Ecology, Restoration and Management: Proceedings of the Arlington Echo Symposium. Gen. Tech. Rep. SRS-91. USDA-Forest Service, Southern Research Station, Asheville, NC. Asheville, NC: USDA Forest Service Southern Research Station, pp 22–30

Horton R, Yohe G, Easterling W, Kates R, Ruth M, Sussman E, Whelchel A, Wolfe D, Lipschultz FC (2014) Northeast. climate change impacts in the united states: the third national climate assessment. US Global Change Research Program, pp 16–1

Hoyt JB (1958) The cold summer of 1816. Ann Assoc Am Geogr 48(2):118–131

Jones PD, Briffa KR, Barnett TP, Tett SFB (1998) High-resolution palaeoclimatic records for the last millennium: interpretation, integration and comparison with General Circulation Model control-run temperatures. Holocene 8:455–471

Kaczka RJ, Wilson R (2021) I-bind: international blue intensity network development working group. Dendrochronologia 68:125859

Kaiser HF (1960) The application of electronic computers to factor analysis. Educ Psychol Measur 20(1):141–151

Kosiba AM, Schaberg PG, Rayback SA, Hawley GJ (2018) The surprising recovery of red spruce growth shows links to decreased acid deposition and elevated temperature. Sci Total Environ 637:1480–1491

Kravitz B, Robock A (2011) Climate effects of high-latitude volcanic eruptions: role of the time of year. J Geophys Res: Atmospheres 116(D1)

Krusic P, Flynt B, Macadeag G, Ladolcetta M, Benjamin J (2015) 25th Annual North American Dendroecological Fieldweek Final Report. Tech. Rep. https://sites.google.com/view/nadef/past-fieldweeks/2015, NADEF, Acadia National Park, Maine

Kunkel KE, Stevens LE, Stevens SE, Sun L, Janssen E, Wuebbles D, Hilberg SD, Timlin MS, Stoecker L, Westcott N et al (2013) Regional climate trends and scenarios for the us national climate assessment part 3. climate of the midwest us. NOAA Technical Report NESDIS 142–3

Larsson L (2014) Coorecorder and cdendro programs of the coorecorder/cdendro package version 7.7

Leland C, D'Arrigo R, Davi N, Anchukaitis K, Andreu-Hayles L, Porter T, Galloway T, Mant M, Wiles G, Wilson R et al (2023) A spatiotemporal assessment of extreme cold in northwestern north america following theunidentified 1809 ce volcanic eruption. Paleoceanography and Paleoclimatology 38(5):e2022PA004581

Lorentzen B (2023) personal communication

Luckman B, Wilson R (2005) Summer temperatures in the canadian rockies during the last millennium: a revised record. Clim Dyn 24(2–3):131–144

Mann ME, Bradley RS, Hughes MK (1999) Northern hemisphere temperatures during the past millennium: inferences, uncertainties, and limitations 26:759–762

Mann ME, Zhang Z, Rutherford S, Bradley RS, Hughes MK, Shindell D, Ammann C, Faluvegi G, Ni F (2009) Global signatures and dynamical origins of the little ice age and medieval climate anomaly. Science 326(5957):1256–1260

Marshall LR, Schmidt A, Johnson JS, Mann GW, Lee LA, Rigby R, Carslaw KS (2021) Unknown eruption source parameters cause large uncertainty in historical volcanic radiative forcing reconstructions. J Geophys Res: Atmospheres 126(13):e2020JD033578

Maxwell RS, Harley GL, Maxwell JT, Rayback SA, Pederson N, Cook ER, Barclay DJ, Li W, Rayburn JA (2017) An interbasin comparison of tree-ring reconstructed streamflow in the eastern united states. Hydrol Process 31(13):2381–2394

Maxwell RS, Belmecheri S, Taylor AH, Davis KJ, Ocheltree TW (2020) Carbonisotope ratios in tree rings respond differently to climatic variations than treering width in a mesic temperate forest. Agric For Meteorol 288:108014

McCarroll D, Pettigrew E, Luckman A, Guibal F, Edouard JL (2002) Blue reflectance provides a surrogate for latewood density of high-latitude pine treerings. Arct Antarct Alp Res 34(4):450–453

McLaughlin S, Downing D, Blasing T, Cook E, Adams H (1987) An analysis of climate and competition as contributors to decline of red spruce in high elevationappalachian forests of the eastern united states. Oecologia 72(4):487–501

Melvin TM, Briffa KR (2008) A "signal-free" approach to dendroclimatic standardisation. Dendrochronologia 26(2):71–86

Neukom R, Barboza LA, Erb MP, Shi F, Emile-Geay J, Evans MN, Franke J, Kaufman DS, Lücke L, Rehfeld K et al (2019) Consistent multidecadal variability in global temperature reconstructions and simulations over the Common Era. Nat Geosci 12(8):643–649

Neukom R, Steiger N, Gómez-Navarro JJ, Wang J, Werner JP (2019) No evidence for globally coherent warm and cold periods over the preindustrial common era. Nature 571(7766):550–554

Oman L, Robock A, Stenchikov G, Schmidt GA, Ruedy R (2005) Climatic response to high-latitude volcanic eruptions. J Geophys Res: Atmospheres 110(D13)

Osman MB, Coats S, Das SB, McConnell JR, Chellman N (2021) North atlantic jet stream projections in the context of the past 1,250 years. Proc Natl Acad Sci 118(38):e2104105118

Patterson T, Maxwell RS, Harley GL, Oliver JS, Speer JH, Collins S, Downe M, Gannon B, Ma L, Raso C et al (2016) Climate—growth relationships of pinusrigida (mill.) at the species' northern range limit, acadia national park, me. Northeastern naturalist 23(4):490–500

Pearl JK, Anchukaitis KJ, Pederson N, Donnelly JP (2017) Reconstructing north eastern united states temperatures using atlantic white cedar tree rings. Environ Res Lett 12(11):114012

Pearl JK, Anchukaitis KJ, Pederson N, Donnelly JP (2020) Multivariate climate field reconstructions using tree rings for the northeastern united states. J Geophys Res: Atmospheres 125(1):e2019JD031619

Pearl JK, Anchukaitis KJ, Donnelly JP, Pearson C, Pederson N, Gaylord MCL, McNichol AP, Cook ER, Zimmermann GL (2020) A late holocene subfossilatlantic white cedar tree-ring chronology from the northeastern united states. Quatern Sci Rev 228:106104

Pederson N, Cook ER, Jacoby GC, Peteet DM, Griffin KL (2004) The influence of winter temperatures on the annual radial growth of six northern range margin tree species. Dendrochronologia 22(1):7–29

Rao MP, Cook ER, Cook BI, Anchukaitis KJ, D'Arrigo RD, Krusic PJ, LeGrande AN (2019) A double bootstrap approach to superposed epoch analysis to evaluate response uncertainty. Dendrochronologia 55:119–124

Rayner N, Parker DE, Horton E, Folland CK, Alexander LV, Rowell D, Kent EC, Kaplan A (2003) Global analyses of sea surface temperature, sea ice, and night marine air temperature since the late nineteenth century. J Geophys Res: Atmospheres 108(D14)

Robeson SM, Maxwell JT, Ficklin DL (2020) Bias correction of paleoclimatic reconstructions: a new look at 1,200+ years of upper colorado river flow. Geophys Res Lett 47(1):e2019GL086689

Robock A (2000) Volcanic eruptions and climate. Rev Geophys 38(2):191–219

Schneider DP, Ammann CM, Otto-Bliesner BL, Kaufman DS (2009) Climate response to large, high-latitude and low-latitude volcanic eruptions in the com-munity climate system model. J Geophys Res: Atmospheres 114(D15)

Seftigen K, Fuentes M, Ljungqvist FC, Björklund J (2020) Using blue intensityfrom drought-sensitive pinus sylvestris in fennoscandia to improve reconstruction of past hydroclimate variability. Clim Dyn 55(3):579–594

Self S, Rampino MR, Barbera JJ (1981) The possible effects of large 19th and 20th century volcanic eruptions on zonal and hemispheric surface temperatures. J Volcanol Geoth Res 11(1):41–60

Sheppard PR, Graumlich LJ, Conkey LE (1996) Reflected-light image analysis ofconifer tree rings for reconstructing climate. The Holocene 6(1):62–68

Sigl M, McConnell JR, Layman L, Maselli O, McGwire K, Pasteris D, Dahl-JensenD Steffensen JP, Vinther B, Edwards R et al (2013) A new bipolar ice core record of volcanism from wais divide and neem and implications for climateforcing of the last 2000 years. J Geophys Res: Atmospheres 118(3):1151–1169

Sigl M, Winstrup M, McConnell JR, Welten KC, Plunkett G, Ludlow F, Büntgen U, Caffee M, Chellman N, Dahl-Jensen D, Fischer H, Kipfstuhl S, Kostick C, Maselli OJ, Mekhaldi F, Mulvaney R, Muscheler R, Pasteris DR, Pilcher JR, Salzer M, Schüpbach S, Steffensen JP, Vinther BM, Woodruff TE (2015) Timing and climate forcing of volcanic eruptions for the past 2,500 years. Nature 523(7562):543–549. https://doi.org/10.1038/nature14565

Stern RL, Schaberg PG, Rayback SA, Murakami PF, Hansen CF, Hawley GJ (2021) Eastern white pine and eastern hemlock growth: possible tradeoffs inresponse of canopy trees to climate. Can J For Res 51(12):1926–1938

Stothers RB (1984) The great tambora eruption in 1815 and its aftermath. Science 224(4654):1191–1198

Tardif J, Brisson J, Bergeron Y (2001) Dendroclimatic analysis of Acer saccharum, Fagus grandifolia, and Tsuga canadensis from an old-growth forest, southwestern Quebec. Can J For Res 31(9):1491–1501

Timmreck C, Toohey M, Zanchettin D, Brönnimann S, Lundstad E, Wilson R (2021) The unidentified eruption of 1809: a climatic cold case. Climate of the Past 17(4):1455–1482

Toohey M, Sigl M (2017) Volcanic stratospheric sulfur injections and aerosol optical depth from 500 bce to 1900 ce. Earth System Science Data 9(2):809–831

Toohey M, Krüger K, Schmidt H, Timmreck C, Sigl M, Stoffel M, Wilson R (2019) Disproportionately strong climate forcing from extratropical explosive volcanic eruptions. Nat Geosci 12(2):100–107

Trinies CA, Bunn AG, Robertson CS, Anchukaitis KJ (2022) Dendroclimatology of yellow-cedar (callitropsis nootkatensis) and temperature variability on the western slopes of the north cascades in washington state, usa, from 1333 to 2015 ce. Tree-Ring Research 78(2):113–128

Trouet V, Babst F, Meko M (2018) Recent enhanced high-summer north atlantic jet variability emerges from three-century context. Nat Commun 9(1):180

Vose R, Easterling DR, Kunkel K, LeGrande A, Wehner M (2017) Temperature changes in the united states. Climate science special report: Fourth national climate assessment 1(GSFC-E-DAA-TN49028)

Wahl ER, Ammann CM (2007) Robustness of the Mann, Bradley, Hughes reconstruction of northern hemisphere surface temperatures: examination of criticisms based on the nature and processing of proxy climate evidence. Clim Change 85(1):33–69

Wang F, Arseneault D, Boucher E, Gennaretti F, Yu S, Zhang T (2022) Tropical volcanoes synchronize eastern canada with northern hemisphere millennial temperature variability. Nat Commun 13(1):5042

Wigley TML, Briffa KR, Jones PD (1984) On the average value of correlated time series, with applications in dendroclimatology and hydrometeorology. J Climate Appl Meteorol 23:201–213

Wiles G, Charlton J, Wilson RJ, DArrigo R, Buma B, Krapek J, Gaglioti BV, Wiesenberg N, Oelkers R (2019) Yellow-cedar blue intensity tree ring chronologies as records of climate, juneau, alaska, usa. Canadian Journal of Forest Research (ja)

Williams PD, Joshi MM (2013) Intensification of winter transatlantic aviation turbulence in response to climate change. Nat Clim Chang 3(7):644–648

Wilson R, Anchukaitis K, Briffa KR, Büntgen U, Cook E, D'arrigo R, Davi N, Esper J, Frank D, Gunnarson B et al (2016) Last millennium Northern Hemisphere summer temperatures from tree rings: part I: the long term context. Quatern Sci Rev 134:1–18

Wilson R, Anchukaitis K, Andreu-Hayles L, Cook E, D'Arrigo R, Davi N, Haberbauer L, Krusic P, Luckman B, Morimoto D et al (2019) Improved dendroclimatic calibration using blue intensity in the southern Yukon. The Holocene 29(11):1817–1830

Wilson R, D'Arrigo R, Andreu-Hayles L, Oelkers R, Wiles G, Anchukaitis K, Davi N (2017) Experiments based on blue intensity for reconstructing north pacific temperatures along the gulf of alaska. Climate of the Past

Wilson R, D'Arrigo R, Buckley B, Büntgen U, Esper J, Frank D, Luckman B, Payette S, Vose R, Youngblut D (2007) A matter of divergence: tracking recent warming at hemispheric scales using tree ring data. J Geophys Res: Atmospheres 112(D17)

Wise EK, Dannenberg MP (2014) Persistence of pressure patterns over north america and the north pacific since ad 1500. Nat Commun 5(1):4912

Zheng Y, Shen H, Abernethy R, Wilson R (2023) Experiments of the efficacy of tree ring blue intensity as a climate proxy in central and western china. Biogeosciences 20(16):3481–3490

Authors and Affiliations

Grant L. Harley[1] [iD] **· Justin T. Maxwell[2] · Karen E. King[3] · Shelly A. Rayback[4] ·
Edward R. Cook[5] · Christopher Hansen[6] · R. Stockton Maxwell[7] · Frederick Reinig[8] ·
Jan Esper[8,9] · Tsun Fung Au[10,11] · Ellen V. Bergan[1] · Katherine E. Brings[1] ·
Nick Koenig[1] · Benjamin Lockwood[12] · Richard D. Thaxton[1]**

✉ Grant L. Harley
gharley@uidaho.edu

Justin T. Maxwell
maxweljt@indiana.edu

Karen E. King
kking@utk.edu

Shelly A. Rayback
srayback@uvm.edu

Edward R. Cook
drdendro@ldeo.columbia.edu

Christopher Hansen
Christopher.hansen@uvm.edu

R. Stockton Maxwell
rmaxwell2@radford.edu

Frederick Reinig
reinig@geo.uni-mainz.de

Jan Esper
esper@uni-mainz.de

Tsun Fung Au
tomau@umich.edu

Ellen V. Bergan
evbergan@uidaho.edu

Katherine E. Brings
kbrings@uidaho.edu

Nick Koenig
koen2388@vandals.uidaho.edu

Benjamin Lockwood
bzl5564@psu.edu

Richard D. Thaxton
thax7738@vandals.uidaho.edu

[1]   Department of Earth and Spatial Sciences, University of Idaho, Moscow, ID 83843, USA

[2]   Department of Geography, Indiana University, Bloomington, IN, USA

[3]   Department of Geography and Sustainability, University of Tennessee, Knoxville, TN, USA

[4]   Department of Geography and Geosciences, University of Vermont, Burlington, VT, USA

[5]   Lamont-Doherty Earth Observatory, Columbia University, Palisades, NY, USA

[6]   Rubenstein School of the Environment and Natural Resources, University of Vermont, Burlington, VT, USA

[7]   Department of Geospatial Science, Radford University, Radford, VA, USA

[8]   Department of Geography, Johannes Gutenberg University, Mainz, Germany

9   Global Change Research Institute of the Czech Academy of Sciences, Brno, Czech Republic

10   Institute for Global Change Biology, University of Michigan, Ann Arbor, MI, USA

11   Department of Ecology and Evolutionary Biology, University of Michigan, Ann Arbor, MI, USA

12   Department of Ecosystem Science and Management, Pennsylvania State University, State College, PA, USA